The article has been published in Journal of Alloys and Compounds

Volume 710, 5 July 2017, Pages 762–770

Zn Vacancy Formation, Zn Evaporation and Decomposition of ZnSb at Elevated Temperatures: Influence on the Microstructure and the Electrical Properties

Authors and affiliations:

Xin Song[1 *], Matthias Schrade[1], Nahum Masó[2], Terje G. Finstad[1]

[1] Department of Physics, University of Oslo, P.O.Box 1048 Blindern, 0316 Oslo, Norway

[2] Department of Chemistry, University of Oslo, P.O.Box 1033 Blindern, 0315 Oslo, Norway

* email: xins@fys.uio.no

Abstract

The influence of annealing on the microstructure and electrical properties of undoped polycrystalline ZnSb samples has been investigated by different experimental techniques. *In situ* XRD in an argon atmosphere showed that ZnSb powders decompose at 300 °C, which is attributed to Zn evaporation. *In situ* SEM in a moist atmosphere showed fast surface deterioration at 450 °C and above, reflecting decomposition of ZnSb and the formation of metallic Sb precipitates. The rate of Zn loss in a reducing atmosphere was determined by thermogravimetry and related to the Zn partial vapor pressure. The increase of the hole carrier concentration of ZnSb measured at room temperature after heat treatment was correlated with Zn evaporation at elevated temperature. The carrier concentration after annealing at 400 °C is consistent with an activation energy for Zn vacancy formation of 0.4 eV and a maximum Zn deficiency x of $Zn_{1-x}Sb$ of 1×10^{-3}.

Keywords: zinc antimonide, thermal stability, evaporation, vacancy formation, thermoelectric material

1. Introduction

The intermetallic Zn-Sb system has recently attracted research interest, as it shows promising thermoelectric performance at intermediate temperatures [1-5]. Unlike other state-of-the-art thermoelectric materials, zinc antimonides consist of neither toxic nor expensive elements [6]. Among several zinc antimonides compositions, ZnSb exhibits a good power factor while the thermal conductivity can be lowered by nanostructuring, giving it promising thermoelectric properties [5, 7-11]. There are currently also other applications of ZnSb actively being explored such as electrodes for rechargeable Li ion batteries [12] or as phase change memory cells [13]. Some research groups have reported the figure of merit zT > 1 in *p*-type ZnSb by various dopants and doping concentration [9, 14]. Experimental studies on nominally undoped ZnSb always show *p*-type behavior, which is usually associated with Zn vacancies being the most stable defect and acting as acceptor species [15-18]. However, there is a lack of available knowledge about the thermal stability of the material. This is naturally of importance for synthesis, applications as well as for characterization at high temperatures.

There are several reports on the observation of the secondary phase Sb [19-21] in ZnSb, usually suspected as a consequence of high temperature treatment. However, detailed and systematic studies are lacking.

There are several possible processes that can affect the stability, among which we here investigate the decomposition of the ZnSb accompanied by Zn evaporation and Sb precipitates. Zn evaporation can be described according to different processes. For simplicity we consider the main processes being

i) the creation of Zn vacancies, while maintaining the ZnSb phase

$$\mathrm{ZnSb(s)} \rightarrow \mathrm{Zn_{1-x}Sb(s)} + x \cdot \mathrm{Zn(g)} \qquad (1)$$

ii) the decomposition of ZnSb, resulting in the formation of a metallic Sb phase

$$\mathrm{Zn_{1-x}Sb(s)} \rightarrow \mathrm{Sb(s)} + \mathrm{Zn(g)} \qquad (2)$$

By combining scanning electron microscopy (SEM), X-ray diffraction (XRD), and thermogravimetry (TG), Zn evaporation can be observed *in situ*. In this paper, we establish the combined occurrence of Eqs. (1) and (2), and study the decomposition of ZnSb as a function of time and temperature in different surrounding atmospheres. We finally relate our measurements of weight loss to Zn vacancy

concentrations and changes in electrical properties. We discuss this in terms of the maximum Zn deficiency of ZnSb and Zn vacancy formation energies.

2. Experimental methods

2.1. Sample synthesis

The ZnSb samples were synthesized by solidification of the melt of stoichiometric proportions (1:1) of Zn (99.99%, Sigma Aldrich) and Sb (99.99%, Alfa Aesar) in an evacuated quartz tube, followed by quenching in water. The ingots were annealed at 490 °C for 100 hours in order to obtain equilibrated and homogenized samples. The resulting pieces were ground into fine powder by ball milling under argon atmosphere for 30 min. For powder X-ray diffraction, the resulting powder was used, while for the other experiments the powder was hot-pressed into pellets at various sintering temperatures from 300 °C to 500 °C for 30 min. at 20 MPa, using a custom built hot-press as described in Ref. [10]. The density was measured by the Archimedes method, according the ISO 5017 standard. The investigations described in the following were carried out on samples sintered at 500 °C unless otherwise noted.

2.2. Structural Characterization

In situ powder X-ray Diffraction (XRD) was done using a Bruker D8 Advance XRD at temperatures from 50 °C to 350 °C under an argon atmosphere (N 5.0, impurity level < 10 ppm). The heating rate was 5 K/min, with 20 min. waiting time before each run to ensure temperature stability. The 2θ scan ranged from 5 degrees to 125 degrees, with a step size of 0.010 degrees at a rate of 5 steps per second. The XRD scan at each temperature thus took 60 min.

The hot-pressed pellets were investigated by scanning electron microscopy (SEM). A FEI Quanta200 FEG - ESEM with a high temperature stage was used for studying the microstructural evolution *in situ* under 50 mbar of water vapor. A Hitachi TM3000 equipped with energy dispersion spectroscopy (EDS) was used to examine the phase composition of the samples.

2.3. Thermogravimetric analysis

Thermogravimetric analysis of the rate of Zn evaporation was performed using a CI Electronics MK2 microbalance. The sample and the counterweight were attached to the arms of the balance with thin platinum wires. The sample was hanging in an alumina tube in a vertical tubular furnace and the

counterweight was hanging in a quartz tube kept at room temperature. The measurement chamber was continuously flushed with argon gas containing approximately 0.1 vol. % H_2 (H-Ar ambient) to prevent oxidation.

The weight change was monitored versus time at different temperatures to obtain the evaporation rate. Due to the rapid mass loss at higher temperatures, short times were needed to extract a reliable mass loss rate under these conditions. All weight measurement values were corrected for buoyancy arising from the asymmetrical density and temperature of the sample and the counterweight.

2.4. Heat treatment

Pellet samples were annealed at 400 °C for 30 min. in either a H-Ar ambient or in a dynamic vacuum in order to examine the influence of heat treatment on the electrical properties. Heating rates for H-Ar ambient and dynamic vacuum were 12 K/min and 20 K/min respectively, depending on the characteristics of the used furnaces. Subsequent cooling from 400 °C to room temperature took around three hours in both furnaces.

2.5. Electrical Properties

The room temperature resistivity was determined by van der Pauw measurements in a custom made set-up, while the carrier concentration was measured by Hall measurements by applying a permanent magnet with B = 1.02 T to the same set-up.

3. Results and discussions

3.1. Hot-pressing of ZnSb : Sb segregation

Fig. 1 shows the relative density of hot-pressed pellets as a function of hot-pressing temperature, surface structure at selected temperatures and a XRD pattern for phase identification. It is observed in Fig. 1(a) that for the specified hot-press and parameters, a temperature above 400 °C was required to obtain a ZnSb pellet with a relative density higher than 95%. The pellet samples sintered at 400 °C and lower temperatures indicated a surface that was rough (here only the sample sintered at 400 °C is shown in Fig. 1 (b)) and no secondary phases were identified by XRD and EDS analyses. For the higher sintering temperatures, such as 500 °C, one could observe precipitates as white dots as seen in Fig. 1(c) which have been identified as Sb by EDS. The microstructures of all the samples in Fig. 1(a) are shown in the supplementary material. The XRD diffractogram of the sample in Fig. 1(c) is

represented by Fig. 1(d). All the peaks belong to the common orthorhombic ZnSb phase. So the amount of Sb was too small to be detected by standard XRD analysis in these samples. Similar findings to these were recently reported by Eklöf *et al.* [19].

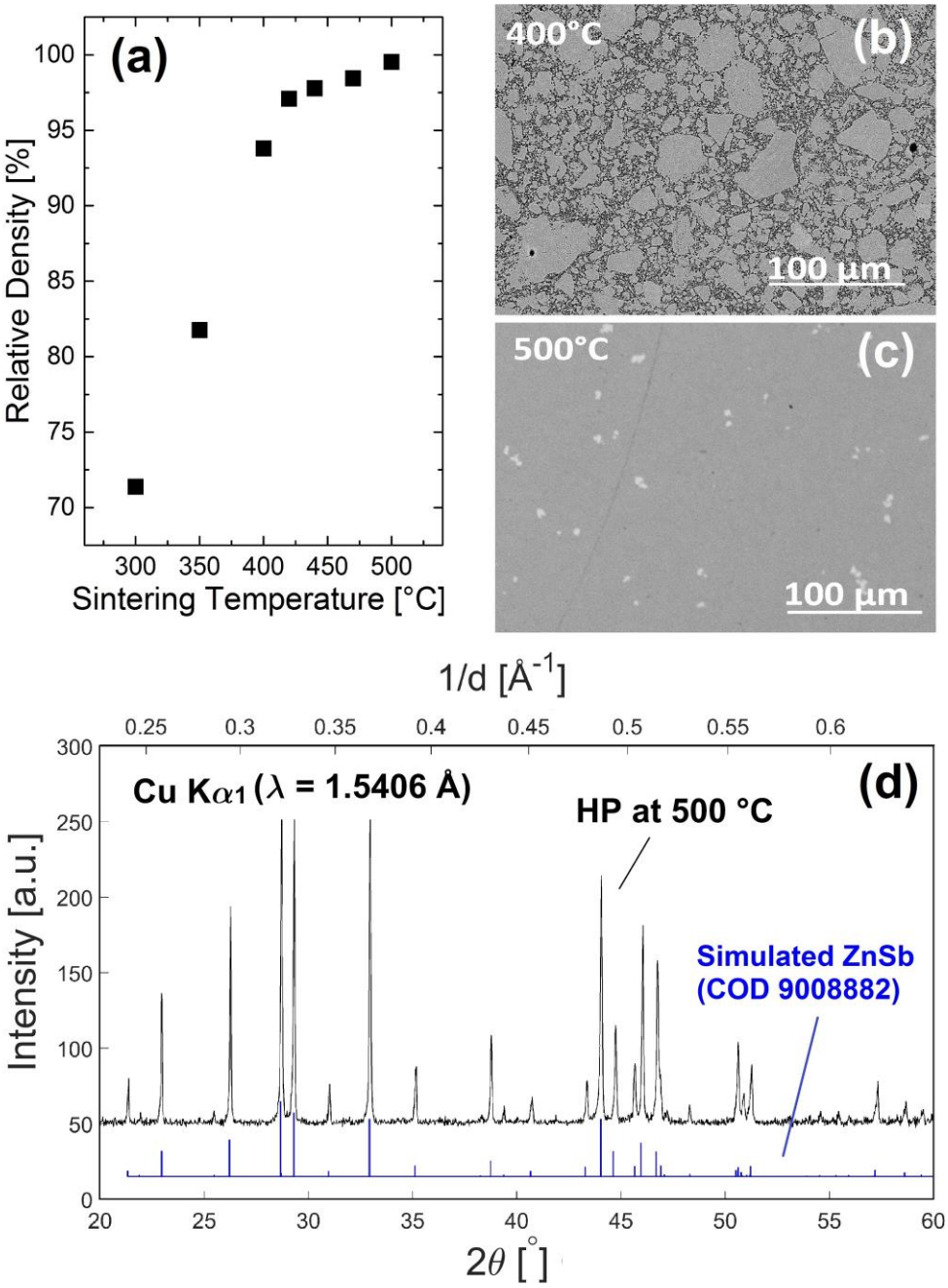

Fig.1 Hot-pressed ZnSb samples **(a)** volumetric density of the samples versus sintering temperature. For ZnSb samples sintered at temperatures lower than 400 °C, the microstructure shows high porosity, as shown in the SEM micrograph in **(b)**; for samples sintered at high temperature, for instance 500 °C as shown in **(c)**, the sample's relative density reaches 99 %. The formation of Sb phase in the sample sintered at 500 °C is also observed as white dots in the SEM imaging. **(d)** is the XRD diffractogram of the sample in **(c).** All the peaks are indexed as ZnSb. However, no Sb phase can be detected by XRD, indicating a Sb concentration below the detection limit.

3.2. *In situ* XRD on ZnSb Powder

In order to investigate the effect of temperature on the phase stability of ZnSb under different conditions, we performed a temperature dependent XRD study on a powder sample. The individual diffractograms were taken during slow heating from room temperature up to 350 °C and subsequent cooling down. For clarity, only the 2θ range from 20° to 24° is shown in Fig. 2. A scan from 20° to 60° can be found in the supplementary material.

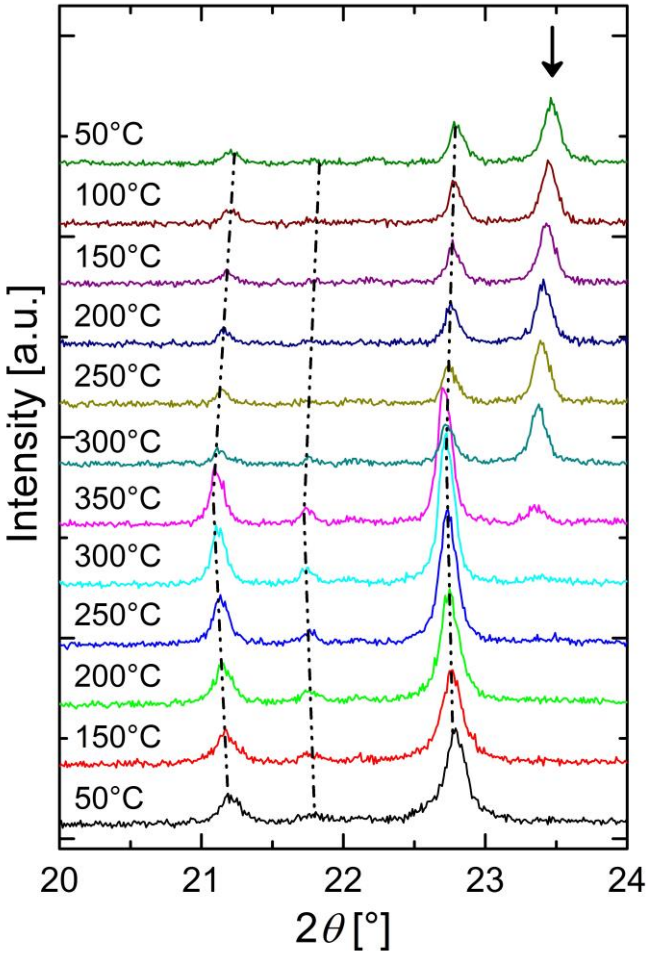

Fig.2 X-ray diffractograms of ZnSb taken during heating, starting at the bottom of the figure, followed by cooling down again. Peaks assigned to the ZnSb are connected by dashed lines as guide to the eye. At temperatures of 300 °C and above, reflections assigned to metallic Sb are indicated by arrows. At the same time as the Sb peak get stronger, the ZnSb peaks get weaker. This is attributed to decomposition of ZnSb by evaporation of Zn(g) and precipitation of Sb . The process is not reversible upon cooling.

The powder used in the present XRD run was slightly Zn rich compared to stoichiometric ZnSb, evidenced by the presence of ZnSb and Zn_4Sb_3 in the initial XRD diffractogram at room temperature: the main peaks can be indexed as ZnSb reflections, while there are weak reflections in addtion that can be attributed to small amounts of Zn_4Sb_3 phase [22, 23]. The Zn_4Sb_3 peaks became weaker upon heating until they disappeared at 250°C. Similar changes in composition have been observed by Mozharivskyj [23] and can be attributed to the lower thermal stability of Zn_4Sb_3 as compared to ZnSb.

Upon heating to 350°C, the ZnSb reflections increasingly sharpened, probably due to grain growth during annealing [10]. At 300°C, additional reflections started to appear, which can be assigned to metallic Sb. Simultaneously, the intensity of the ZnSb peaks became weaker. The intensity changes were non-reversible upon cooling. We think that this behavior is an indication of Zn evaporation and decomposition of ZnSb into $Zn_{1-x}Sb$ and metallic Sb, which is in agreement with previous reports [23, 24] and similar to the phase relations of the samples sintered at different temperatures. However, also oxidation of ZnSb and the creation of ZnO could lead to a precipitation of excess Sb. By XRD, we have observed a small amount of ZnO at 300°C. This is possibly due to purity of the controlled gas we have used, which could provide spurious oxygen and thereby it oxidizes the sample. Therefore, one could argue the segregation of Sb is due to the formation of ZnO instead of Zn evaporation. However, the ZnO peak intensity is very low compared to the increasing of Sb peak intensity, indicating that there is a certain amount of Zn loss. We conclude that oxidation was not dominating in the Sb segregation process. In comparison with the sintered pellet samples, the degree of decomposition for the powder sample was much larger and the onset temperature was considerably lower.

3.3. *In situ* SEM on hot-pressed pellets

In parallel to the XRD investigation, we studied the influence of annealing and Zn evaporation on the microstructure of a pellet sample of ZnSb. For this purpose, a dense sample sintered at 500 °C was used to study Zn evaporation *in situ* in a SEM equipped with a high temperature stage operated in a wet atmosphere. Secondary electron images of the sample surface at different temperatures and times are shown in Fig. 3. No changes were observed up to 400°C, whereas at 450°C, the surface degraded rapidly. Phase analysis by EDS and backscattered electron imaging was performed at room temperature before and after the heat treatment and is shown in Fig. 4. Initially, small grains of the Sb phase were evenly distributed over the surface, shown as the bright spots in Fig. 4 (a). The heat treated sample showed many pores of typically 5 × 20 μm^2 in lateral dimension, which were decorated with Sb-rich areas as seen in Fig. 4 (c). We note that we have not observed such severe decomposition of ZnSb by heat treatments at similar temperatures in vacuum or in a H-Ar atmosphere and, consequently, the decomposition could be influenced by the wet atmosphere (p_{H2O} ~ 50 mbar) used for imaging purposes and/or by gas ions and radicals being created by the electron beam. Further studies are needed to identify the source of the enhanced degradation.

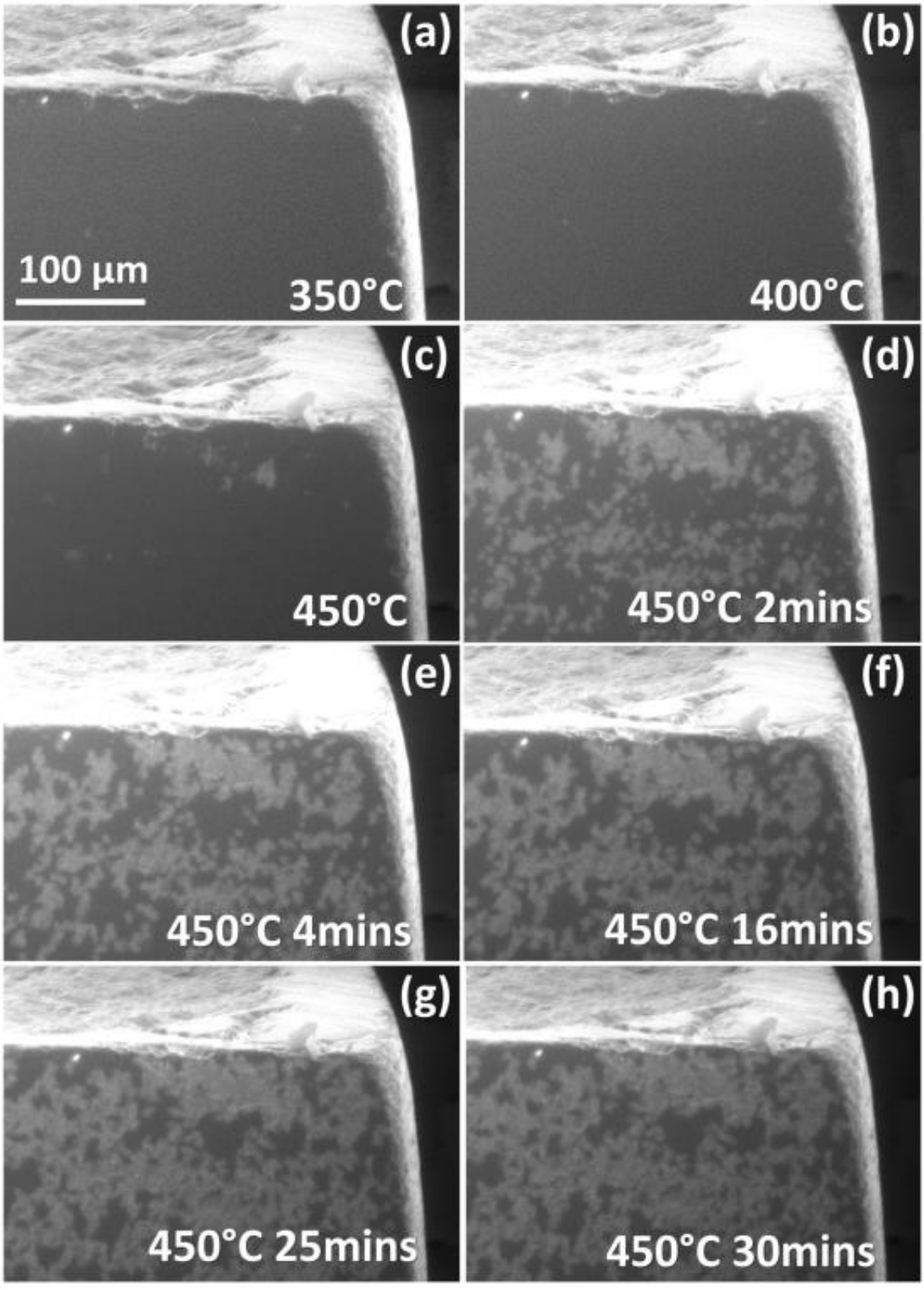

Fig.3 Secondary electron SEM images of a hot-pressed ZnSb sample in moist atmosphere. **(a) - (c)** at different temperatures as indicated. **(d) - (h)** At 450 °C the evolution of the surface was studied as a function of time.

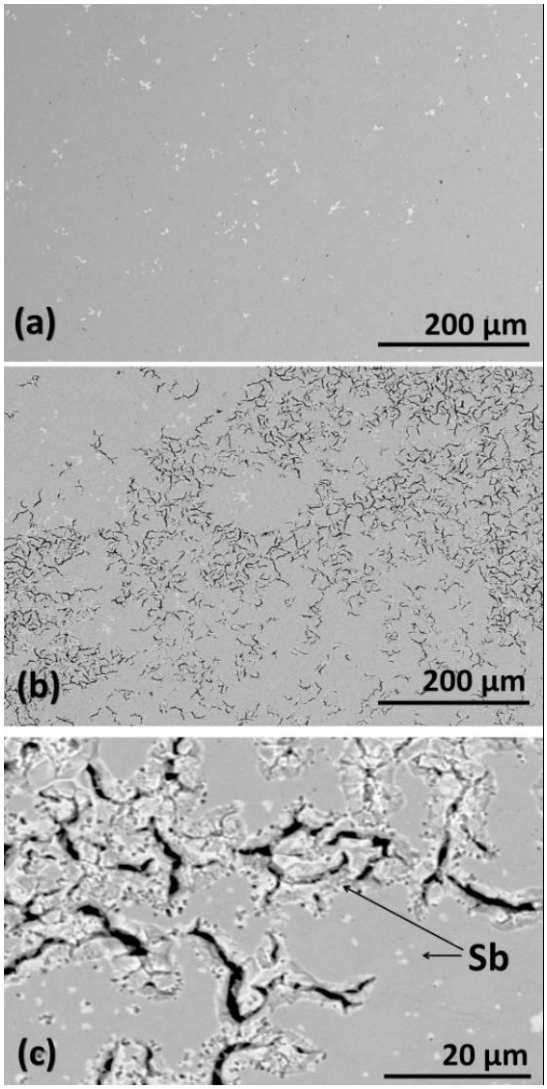

Fig.4 Backscattered electron images of the sample shown in Fig. 3 before and after heat treatment. **(a)** The as-sintered sample shows a smooth surface with bright evenly distributed Sb inclusions. **(b)** The surface after a heat treatment at 450 °C for 30 min. Microscopic pores have formed throughout the surface. **(c)** The pores are decorated with metallic Sb, consistent with the evaporation of Zn.

3.4. Thermogravimetric results

The indications of Zn evaporation observed by the structural characterization techniques can be confirmed and quantified by weight loss experiments, i.e. thermogravimetry. The measurement of the sample weight during annealing as a function of time did not only yield the total amount of Zn loss, but also provided insight into the thermodynamics of Zn evaporation as shown in the following where we firstly discuss the relation of thermogravimetry to the equilibrium vapor pressure of a solid material in general.

If a sample was placed in a closed chamber of uniform temperature, once the equilibrium vapor pressure has built up, there would be a detailed balance between evaporation and adsorption of atoms and the associated fluxes. The vapor pressure, *P*, is related to this flux, J_n, by [25]

$$P = \sqrt{2\pi k_B T m} \times J_n \qquad (3)$$

where k_B is the Boltzmann's constant, T is the absolute temperature, and m is the mass of the considered species. If most of the flux of evaporated atoms in the present experiment are transported away from the samples and deposited in regions with a significantly lower temperature, then we could neglect any flux of Zn atoms back to the sample. If the state of the material is assumed to be as under equilibrium, the rate of weight loss, α, is then proportional to the flux of atoms and thereby the vapor pressure:

$$P = \sqrt{\frac{2\pi k_B T}{mA^2}} \times \alpha \qquad (4)$$

where *A* is the surface area of the sample.

Figure 5 (a) shows the weight of a ZnSb sample as a function of time at different temperatures. We attribute the observed weight loss solely to Zn evaporation. At constant temperature, the rate of mass loss is roughly constant, and increases significantly with increasing temperature. In Fig. 5 (b) we show $\sqrt{T} \times \alpha$, which is proportional to the vapor pressure *P*, for different temperatures in an Arrhenius plot. The $\sqrt{T} \times \alpha$ shows an activated behavior with an activation energy of 1.87 ± 0.02 eV, in good agreement with the result reported by Hirayama (1.74 eV), which was obtained using a Knudsen cell experiment (effusion method) [26]. From the temperature dependence of the mass loss rate (or alternatively of the vapor pressure), one can calculate the formation enthalpy of ZnSb using tabulated thermodynamic parameters, as explained in Ref. [27].

Equation (4) allows, in principle, a direct calculation of the absolute value of *P* from thermogravimetric data, if the evaporating surface area *A* is known. However with a surface area of 1 cm^2 estimated from the geometry of the sample and $m = 65\ g/N_A$ as the mass of a Zn atom, the calculated vapor pressure is roughly two orders of magnitude lower than reported by Hirayama in Ref. [27]. We consider that this is a real discrepancy beyond uncertainties in the measurements. A plausible cause for the underestimation of the vapor pressure by the TG experiment done presently is the assumption of no Zn vapor pressure build-up at the ZnSb surface. The observed weight loss rate α reflects the net flux of atoms from the sample. Therefore, J_n in Eq. (3) calculated from α could be

significantly underestimated, if the flux of Zn atoms back to the sample cannot be neglected, which again results in an underestimated Zn vapor pressure. The gas flow in the measurement cell would probably have been in a laminar flow regime, and we would approximately have a stagnant gas layer at the surface. The Zn vapor would then be transported mostly by diffusion in the gas phase close to the surface. The removal of Zn atoms may then not have been efficient enough to neglect desublimation. A closer match to the values of Ref. [27] may thus have been obtained if the measurements had been done under vacuum conditions. However, the extracted activation energy should still be associated with evaporation, since the diffusion in the gas phase is not an activated process. We could also consider the situation as being close to the equilibrium vapor pressure of ZnSb for the stoichiometry at this state.

Non-uniform surface topography with different evaporation rates could also complicate the situation. It was observed that the erosion of the surface was very non-uniform under the conditions prevailing in the SEM during heating (Figs. 3 and 4). A detailed investigation of surface degradation may lead to viable strategies to reduce Zn evaporation from ZnSb.

We wanted to test if the data extracted from the TG measurement are reasonably consistent with the *in situ* XRD measurements in Fig. 2, which were done in similar atmospheres, but with a powder sample instead of a sintered pellet. In order to test the consistency we extrapolated the mass loss rate α from Fig. 5(b) to 350 °C so that we could calculate the number of evaporated Zn atoms from a ZnSb sphere with diameter d during a certain time, assuming that the evaporation occurred at a constant rate. We have previously reported the mean grain diameter of the ball-milled powder used for the XRD investigation to be around 30 nm at room temperature and increasing to 80 nm at 350 °C [10]. During the XRD measurement, the powder was kept at each temperature for roughly 60 min. (20 min. pause to reach a stable temperature + 40 min. for the XRD sweep). After this time at 350 °C, 5.2×10^6 Zn atoms should be evaporated from an 80 nm grain, corresponding to the evaporation of 90% of the Zn in the grain. This value is in rough agreement with the XRD peak intensity from ZnSb being reduced by more than a factor of two after the 350°C analysis as seen in Fig. 2. We conclude that the observations from XRD experiments are in reasonable agreement with the Zn loss determined from the TG experiments. We also demonstrated the large sensitivity to surface topography.

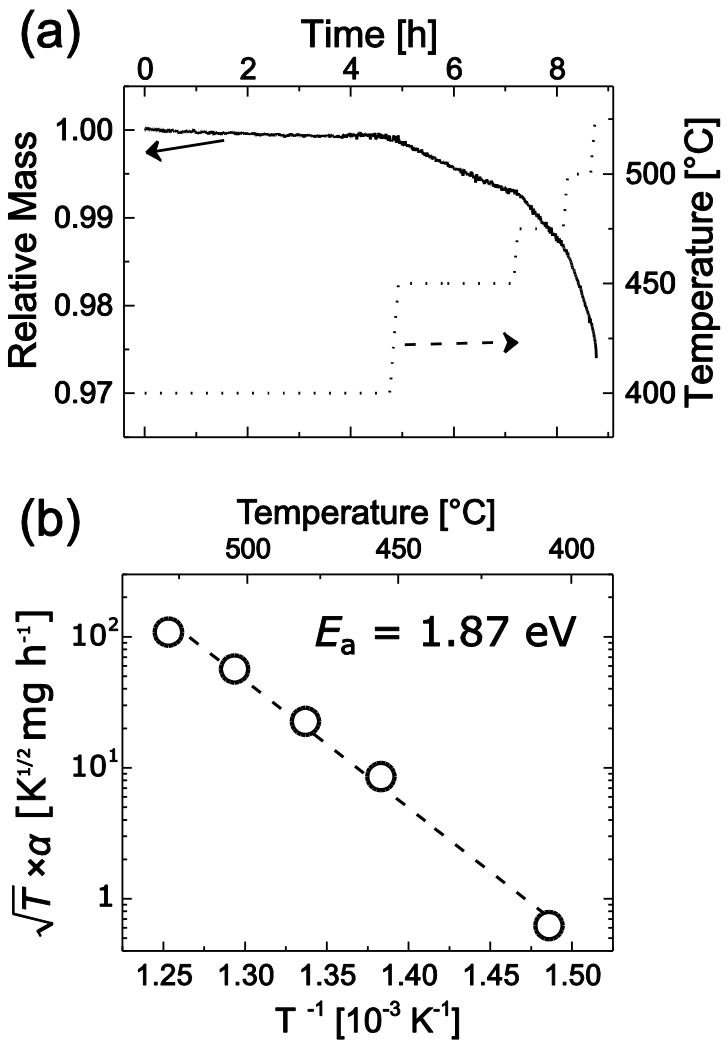

Fig.5 (a) The mass loss of ZnSb as a function of time. The rate $\boldsymbol{\alpha}$ of Zn evaporation is constant at constant temperature $\boldsymbol{T}$, but increases with increasing temperature. **(b)** $\sqrt{\boldsymbol{T}} \times \boldsymbol{\alpha} \propto \boldsymbol{P}$ for different temperatures.

3.5. Overall Discussion and Influence on the Electronic Properties

To check the influence on the electrical properties of heat treatment under similar conditions to those under the TG experiments described above, two hot-pressed ZnSb samples were annealed in H-Ar ambient. To check the influence of the ambient condition during heat treatment another was annealed in dynamic vacuum. The samples were heated to 400 °C in H-Ar ambient (sample #1 and #2) or dynamic vacuum (sample #3), and then kept at this temperature for 30 minutes before cooling down to room temperature. The room temperature electrical conductivity, charge carrier concentration and mobility were measured before and shortly after the annealing. The measured values are tabulated Table 1.

The initial carrier concentration of the samples around 5×10^{18} cm^{-3} is associated with a combination of impurities and defects in the material. After annealing, the carrier concentration p of all samples had

increased, also reflected in an increased conductivity σ, while the carrier mobility $\mu = \frac{\sigma}{ep}$ decreased somewhat.

Table 1. Influence of annealing at 400 °C for 30 minutes in H-Ar ambient (sample #1 and #2) and dynamic vacuum (sample #3) on the electrical properties of ZnSb at room temperature. The carrier concentration increases significantly for all three samples, leading to an increased electrical conductivity $\boldsymbol{\sigma}$.

Sample	Annealing		p [10^{18} cm^{-3}]	σ [S cm^{-1}]	μ [cm^{2}V^{-1}s^{-1}]
#1	H-Ar	Before	7.95	202	159
		After	14.10	262	116
#2	H-Ar	Before	3.57	134	235
		After	10.2	360	220
#3	Vacuum	Before	6.17	221	224
		After	24.1	694	180

In the following, we relate the results in Table 1 to the TG measurements, and discuss these results in the light of available literature data on Zn deficiency and vacancy formation energies in ZnSb. In order to do so we first need to make several simplifying assumptions about the observed electrical property changes and the estimated evaporation from the TG experiment. We will make the following assumptions about the conditions and processes:

A1 :The changes in Table 1 in the electrical properties are due to Zn evaporation and Zn vacancies.

A2: Each Zn vacancy gives rise to one hole carrier in the valence band at room temperature.

A3: The Zn vacancy concentration at 400 °C was instantly "frozen" or quenched as the cool down starts. In other words the vacancy concentration does not follow the equilibrium concentration during cooling down.

Some of these assumptions will be further discussed.

Here, we first discuss sample #1 and #2, as these were annealed under similar conditions as the sample for the TG measurement, so that we can relate the two different experimental observations: the mass loss and the carrier concentration. After annealing, the carrier concentration p of both samples increased by roughly 6×10^{18} cm^{-3}. From the TG analysis, we can estimate the absolute Zn loss during annealing of the samples used for the electrical measurements. After 30 min at 400°C, the relative weight loss was around 1.5×10^{-4}, which corresponds to a Zn deficiency x in $Zn_{1-x}Sb$ of 4×10^{-4}, assuming homogenization during annealing. The atomic density of Zn in ZnSb is 2.05×10^{22} cm^{-3}, so that the observed weight loss corresponds to an increase in the Zn vacancy concentration by 8×10^{18}

cm^{-3}, assuming that Zn evaporates only by the formation of additional vacancies (Eq. 1) and neglecting the potential of decomposition and precipitation of Sb inclusions (Eq. 2). Under these assumptions, the expected increase in the charge carrier concentration of sample #1 and #2 by the heat treatment in H-Ar is 8×10^{18} cm^{-3}, which is very similar to the observed values in sample #1 and #2, thereby supporting our assumptions, in particular A1 and A2.

For sample #3, the increase in carrier concentration was 18×10^{18} cm^{-3} which is larger than the increase observed for #1 and #2. The nominal difference in the heat treatments was the ambience, and the different change in carrier concentration goes in the direction expected. The observation may indicate that the rate and degree of Zn evaporation from ZnSb is in fact very sensitive to the surrounding atmosphere, as noted before in the discussion of *in situ* SEM and TG analysis, and evaporation will be faster under dynamic vacuum than when a stagnant gas layer is present close to the surface.

We also measured the carrier concentration of sample #3 again, after keeping it for several days at room temperature, in order to check to which degree the selected heat treatment procedure yield reversible or irreversible changes for the cooling rates that were used. It is well known that electrically active defects in semiconductors can be involved in processes with a large span in characteristic times and both irreversible and reversible changes involving defects are observed. That applies to ZnSb as well; several authors have reported a hysteresis behavior of the hole carrier concentration (and/or resistivity) upon thermal cycling between a large range of temperatures [5, 28-31]. The slow relaxation back to the initial value at low temperature can have a large range of time constants. Our measurements for sample #3 are shown in figure 6. The measurements can be interpreted as a support for the idea that the heat treatment induced a change that is relatively stable at room temperature for several days. The measurements also indicated that we may reach an apparent equilibrium condition by annealing sample #3 in H-Ac at 400 °C as we argue further on below.

In order to estimate the solubility limit of Zn vacancies in ZnSb at 400 °C under dynamic vacuum conditions, we analyze the carrier concentration of sample #3 after repeated annealing (Fig. 6). The carrier concentration shows a fourfold increase after the first 30 min at 400 °C, while further annealing only leads to a minor increase (20 %), eventually reaching 28×10^{18} cm^{-3}. This may indicate that this value corresponds to the maximum Zn vacancy concentration in ZnSb at 400°C This result can be equivalently expressed as a maximum non-stoichiometry x in $Zn_{1-x}Sb$ of 1×10^{-3} at 400°C.

This calculated value for x of 1×10^{-3} is, however, much smaller than previously reported values of x = 0.04 (by *in situ* XRD at 400°C) [23, 32] or 0.03 (by intentional under-stoichiometry at 380°C) [33].

Note that under assumptions A2 and A3, the previously reported values for *x* would correspond to a vacancy concentration and thereby a room temperature carrier concentration of 6 - 8 × 10^{20} cm^{-3}, which is much larger than any reported measurement on ZnSb.

We may test how our estimated maximum vacancy concentration at 400 °C relates to usual expressions for the vacancy concentration containing the formation energy $\Delta E_{V_{Zn}}$ of a Zn vacancy. The concentration in equilibrium of vacancies at a certain temperature is often given as [25]

$$[V_{Zn}] = [Zn_{Zn}] \times \exp\left(-\frac{\Delta E_{V_{Zn}}}{k_B T}\right) \qquad (5)$$

By substituting the observed increase in the carrier concentration of 18 × 10^{18} cm^{-3} for the vacancy concentration at 400 °C and substituting 2.05 × 10^{22} cm^{-3} for the atomic density of Zn sites, we obtain a vacancy formation energy of 0.4 eV. This value is comparable with the values calculated by Bjerg *et al.* (0.3 ~ 0.5 eV) [16]. On the other hand, a formation energy of 0.8 eV was obtained in a recent DFT study [17], which would lead to a vacancy concentration in the order of 10^{16} cm^{-3}.

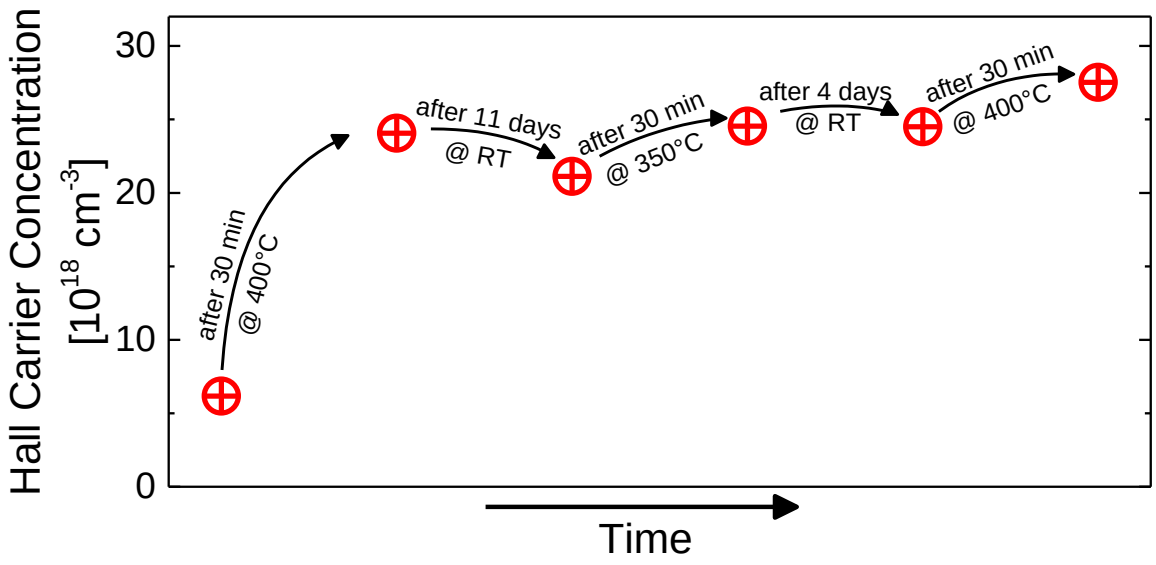

Fig.6 Hall carrier concentration of sample #3 at room temperature (RT) after repeated annealing under dynamic vacuum. The carrier concentration increases, but seems to saturate around 30 × 10^{18} cm^{-3}, which may correspond to the maximum Zn deficiency in ZnSb at 400°C.

3.6. Additional comments

We first make a comment on why the effect of Sb precipitates on the electrical properties can be neglected in the present case. All samples used here for studying the electrical properties were sintered at 500°C, and show the formation of Sb inclusions on the surface as shown in Fig. 1 (f). However, we do not expect the small amount of Sb inclusions to lead to a noticeable change in the electrical

properties of the samples from effective medium considerations combining Sb and ZnSb. Also from the point of view of carrier depletion regions around the Sb particles caused by the ZnSb/Sb interface, the Sb inclusion will have little influence because of the short Debye length in the rather heavy doped ZnSb material ($p > 4 \times 10^{18}$ cm^{-3}); the depletion region is estimated to be 10 nm, or smaller, which is very small compared to the average distance > 10 μm between Sb precipitates, so the depletion region takes up an insignificant portion of the available volume for carriers.

We next make some comments on why we could have an increase in the vacancy concentration for ZnSb samples that had first been sintered (hot-pressed) at 500 °C and then later annealed at 400 °C to induce the increase. We argue here in order to get ahead of common misconceptions. We should not have observed an increase if : i) the vacancy concentration was only a function of the temperature and ii) all temperature treatments were terminated by a very fast quench that 'froze' the vacancy concentration. Since we did measure an increase in the hole concentration by the 400 °C anneal (Table 1 and/or Fig. 6) either the increase represented something else than the vacancy concentration or the assumptions i) and ii) do not hold. It is clear that condition i) does not hold. Eq.(5) gives the vacancy concentration for a particular Zn partial pressure and ambient. The vacancy concentration will obviously depend upon the Zn partial pressure and that can readily be derived from the law of mass action applied to the reaction given by Eq.(1). The ambient and partial pressure of Zn is believed to be quite different for the sintering process than that for the 400 °C anneal. We have not quantified the difference, which would have been desired, thus we don't know the relationship between the vacancy concentrations, for equilibrium conditions. Further we do not know whether equilibrium was reached. Regarding condition ii) above, we have that the cooldown from the hot-press temperature was very slow in comparison with the cooldown from the 400 °C annealing. Given that there is sufficient diffusion for the system to change the vacancy concentration at 400 °C, it indicates that the freezing condition ii) does not apply to the 500 °C hot-press case. Thus the vacancy concentration in the ZnSb after cooldown should be representative of a lower temperature and an ambient of higher Zn partial pressure than that of the anneal treatment. To conclude the argumentation: assumption i) and ii) do not hold, so it is possible that we measure the change in vacancy concentration by the hole concentration and in the current experimental conditions, it is not violating standard thermodynamic trends to observe an increase in vacancy concentration by the specific annealing at 400 °C after hot-pressing at 500 °C. In the different experiments and observations we have presented in this paper, we have showed that the ambient can play a large role for segregation, decomposition, and thus also probably for vacancy formation in ZnSb.

The parameterization of the data by a Zn vacancy formation energy, as shown in the overall discussion, assumed that the vacancy concentration at 400 °C was frozen upon cooling, i.e. that the cooling rate

was so fast that the diffusion- and decomposition- processes could not maintain equilibrium. If the sample was cooled down slowly, the Zn vacancy concentration could follow its thermodynamic equilibrium concentration to significantly lower temperatures, and thereby leading to lower values of the hole carrier concentration. The influence of parameters such as cooling rate and annealing time on the properties of ZnSb could be studied in the future. Our experiments (Fig. 6) indicate, however, that the maximum carrier concentration of 3×10^{19} cm^{-3} is indeed representative of a freezing temperature between 350 °C and 400 °C, so that our rough estimation of the Zn vacancy formation energy is justified for the surface Zn pressure prevailing in the experiments.

The absolute rates of Zn evaporation observed for a given temperature also varied vastly with the ambient of the material. For example ZnSb can be hot-pressed above 500 °C without degradation of the material, while a noticeable decomposition occurs at temperatures as low as 300 °C if the powder is heated directly in argon atmosphere. Apart from the larger surface area and shorter diffusion length in the powder sample that will accelerate the evaporation, the evaporation rate also depends much on the environment, which can be reduced by a build-up of a local Zn vapor pressure. This is further indicated by the possibly two orders of magnitude difference in the rate of mass loss of Zn in the present TG experiment and effusion experiments in the literature.

4. Concluding remarks

In this paper, we have studied the effect of annealing on the microscopic properties of ZnSb. *In situ* XRD experiments under argon flow show that significant Zn evaporation can occur at temperatures above 300 °C, eventually leading to decomposition and the precipitation of metallic Sb inclusions. Severe decomposition and erosion of ZnSb surface was observed by SEM at 450 °C in a moist ambient. The rate of Zn evaporation was quantified using a thermogravimetric method in an H-Ar atmosphere.

Measurements of the room temperature electrical conductivity and carrier concentration pre- and post-annealing were consistent with the assumption that Zn vacancies act as acceptors in ZnSb, making them the most likely cause for the universally observed *p*-type behavior of nominally undoped ZnSb. The observed net charge carrier concentration of ~ 3×10^{19} cm^{-3} in Zn-deficient ZnSb corresponding to a solubility of Zn vacancies x in $Zn_{1-x}Sb$ is in the order of < 10^{-3} at 400 °C, which is significantly lower than that previously reported from structural studies. The measurements are consistent with a formation energy of 0.4 eV for a Zn vacancy under the present conditions at 400 °C.

We finally note that this irreversible evaporation of Zn at elevated temperatures will influence the experimentally observed thermoelectric properties. One needs to be aware of the possibility of Zn

evaporation and decomposition, and taking precautions as required. In order to ensure long term stability of ZnSb in a device operated at elevated temperatures, adequate protective coatings to prevent the slow evaporation of Zn are required and need to be developed in the future.

Acknowledgments

The authors gratefully acknowledge financial support by the Research Council of Norway. X.S. was funded through the project No. 216078 (NanoThermo), M.S. by project No. 228854 (Thelma) and N.M. by project No. 219731 (BioPCFC).

References

[1] Z.-h. Zheng, P. Fan, J.-t. Luo, G.-x. Liang, P.-j. Liu, D.-p. Zhang, Enhanced thermoelectric properties of Cu doped ZnSb based thin films, Journal of Alloys and Compounds, 668 (2016) 8-12.
[2] R. Pothin, R.M. Ayral, A. Berche, D. Granier, F. Rouessac, P. Jund, Preparation and properties of ZnSb thermoelectric material through mechanical-alloying and Spark Plasma Sintering, Chemical Engineering Journal, 299 (2016) 126-134.
[3] K. Valset, X. Song, T.G. Finstad, A study of transport properties in Cu and P doped ZnSb, Journal of Applied Physics, 117 (2015) 045709.
[4] L.V. Prokofieva, P.P. Konstantinov, A.A. Shabaldin, D.A. Pshenai-Severin, A.T. Burkov, M.I. Fedorov, Doping and defect formation in thermoelectric ZnSb doped with copper, Semiconductors, 48 (2014) 1571-1580.
[5] M.I. Fedorov, L.V. Prokof'eva, D.A. Pshenay-Severin, A.A. Shabaldin, P.P. Konstantinov, New Interest in Intermetallic Compound ZnSb, Journal of Electronic Materials, 43 (2014) 2314-2319.
[6] T. Zou, X. Qin, Y. Zhang, X. Li, Z. Zeng, D. Li, J. Zhang, H. Xin, W. Xie, A. Weidenkaff, Enhanced thermoelectric performance of β-Zn_4Sb_3 based nanocomposites through combined effects of density of states resonance and carrier energy filtering, Scientific Reports, 5 (2015) 17803.
[7] C. Okamura, T. Ueda, K. Hasezaki, Preparation of Single-Phase ZnSb Thermoelectric Materials Using a Mechanical Grinding Process, Materials Transactions, 51 (2010) 860-862.
[8] K. Valset, P.H.M. Böttger, J. Taftø, T.G. Finstad, Thermoelectric properties of Cu doped ZnSb containing Zn_3P_2 particles, Journal of Applied Physics, 111 (2012) 023703.
[9] M.I. Fedorov, L.V. Prokofieva, Y.I. Ravich, P.P. Konstantinov, D.A. Pshenay-Severin, A.A. Shabaldin, Thermoelectric efficiency of intermetallic compound ZnSb, Semiconductors, 48 (2014) 432-437.
[10] X. Song, K. Valset, J.S. Graff, A. Thøgersen, A.E. Gunnæs, S. Luxsacumar, O.M. Løvvik, G.J. Snyder, T.G. Finstad, Nanostructuring of Undoped ZnSb by Cryo-Milling, Journal of Electronic Materials, 44 (2015) 2578-2584.
[11] X. Song, T.G. Finstad, Review of Research on the Thermoelectric Material ZnSb, in: Thermoelectrics for Power Generation - A Look at Trends in the Technology, InTech, Rijeka, 2016, pp. Ch. 6.
[12] S. Saadat, Y.Y. Tay, J. Zhu, P.F. Teh, S. Maleksaeedi, M.M. Shahjamali, M. Shakerzadeh, M. Srinivasan, B.Y. Tay, H.H. Hng, J. Ma, Q. Yan, Template-Free Electrochemical Deposition of Interconnected ZnSb Nanoflakes for Li-Ion Battery Anodes, Chemistry of Materials, 23 (2011) 1032-1038.
[13] G. Wang, X. Shen, Y. Lu, S. Dai, Q. Nie, T. Xu, Investigation on pseudo-binary ZnSb-Sb_2Te_3 material for phase change memory application, Journal of Alloys and Compounds, (2015) 341-346.
[14] D.-B. Xiong, N.L. Okamoto, H. Inui, Enhanced thermoelectric figure of merit in *p*-type Ag-doped ZnSb nanostructured with Ag_3Sb, Scripta Materialia, 69 (2013) 397-400.
[15] P.H.M. Böttger, G.S. Pomrehn, G.J. Snyder, T.G. Finstad, Doping of p-type ZnSb: Single parabolic band model and impurity band conduction, physica status solidi (a), 208 (2011) 2753-2759.
[16] L. Bjerg, G.K.H. Madsen, B.B. Iversen, Ab initio Calculations of Intrinsic Point Defects in ZnSb, Chemistry of Materials, 24 (2012) 2111-2116.
[17] P. Jund, R. Viennois, X. Tao, K. Niedziolka, J.-C. Tédenac, Physical properties of thermoelectric zinc antimonide using first-principles calculations, Physical Review B, 85 (2012) 224105.
[18] X. Song, P.H.M. Böttger, O.B. Karlsen, T.G. Finstad, J. Taftø, Impurity band conduction in the thermoelectric material ZnSb, Physica Scripta, 2012 (2012) 014001.
[19] D. Eklof, A. Fischer, Y. Wu, E.W. Scheidt, W. Scherer, U. Haussermann, Transport properties of the II-V semiconductor ZnSb, Journal of Materials Chemistry A, 1 (2013) 1407-1414.
[20] A.B. Blichfeld, B.B. Iversen, Fast direct synthesis and compaction of phase pure thermoelectric ZnSb, Journal of Materials Chemistry C, 3 (2015) 10543-10553.
[21] R. Pothin, R.-M. Ayral, A. Berche, F. Rouessac, P. Jund, Interest of the differential thermal analysis on the characterization of a thermoelectric material: ZnSb, Journal of Alloys and Compounds, 657 (2016) 358-365.
[22] Y. Mozharivskyj, Y. Janssen, J.L. Harringa, A. Kracher, A.O. Tsokol, G.J. Miller, Zn13Sb10: A Structural and Landau Theoretical Analysis of Its Phase Transitions, Chemistry of Materials, 18 (2006) 822-831.
[23] Y. Mozharivskyj, A.O. Pecharsky, S. Bud'ko, G.J. Miller, A Promising Thermoelectric Material: Zn_4Sb_3 or $Zn_{6-\delta}Sb_5$. Its Composition, Structure, Stability, and Polymorphs. Structure and Stability of $Zn_{1-\delta}Sb$, Chemistry of Materials, 16 (2004) 1580-1589.

[24] A. Fischer, E.W. Scheidt, W. Scherer, D.E. Benson, Y. Wu, D. Eklöf, U. Häussermann, Thermal and vibrational properties of thermoelectric ZnSb: Exploring the origin of low thermal conductivity, Physical Review B, 91 (2015) 224309.
[25] S.A. Campbell, The Science and Engineering of Microelectronic Fabrication, Oxford University Press Inc., 1996.
[26] C. Hirayama, Vaporazation of Zinc Antimonide, Thermoelectricity, Quarterly progress report no. 2, DTIC datebase, Defense Technical Information Center, (1962).
[27] C. Hirayama, The Dissociation Pressure of Zinc Antimonide, Journal of The Electrochemical Society, 110 (1963) 88-91.
[28] P.J. Shaver, J. Blair, Thermal and Electronic Transport Properties of *p*-Type ZnSb, Physical Review, 141 (1966) 649-663.
[29] N.L. Kostur, V.I. Psarev, Electrical properties of doped single crystals of ZnSb, Soviet Physics Journal, 10 (1967) 21-23.
[30] S.A.A.a.P.e.L.V.a.K.P.P.a.B.A.T.a.F. M.I., Acceptor impurity of copper in ZnSb thermoelectric, Materials Today: Proceedings, 2 (2015) 699 – 704
[31] L.V. Prokofieva, P.P. Konstantinov, A.A. Shabaldin, On the tin impurity in the thermoelectric compound ZnSb: Charge-carrier generation and compensation, Semiconductors, 50 (2016) 741-750.
[32] Z.M. Gibbs, H.-S. Kim, H. Wang, G.J. Snyder, Band gap estimation from temperature dependent Seebeck measurement-Deviations from the 2e|S|maxTmax relation, Applied Physics Letters, 106 (2015) 022112.
[33] Q. Guo, S. Luo, Improved thermoelectric efficiency in *p*-type ZnSb through Zn deficiency, Functional Materials Letters, 08 (2015) 1550028.

Supplementary 1

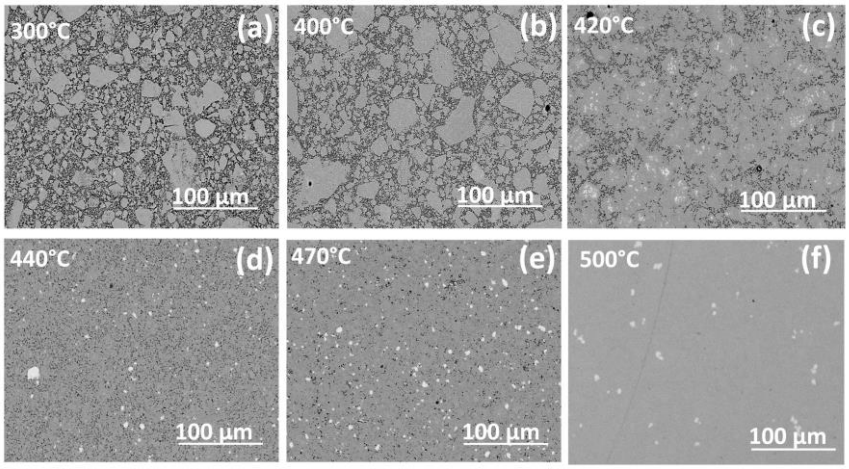

Fig. S1 ZnSb samples sintered (hot-pressed) at different temperatures

For temperatures below 400 °C no secondary phase can be observed for the used process parameters, while the relative density reaches 95 %. At higher sintering temperatures, the density increases further, and the formation of Sb phase is observed as white dots in the SEM micrograph.

Supplementary 2

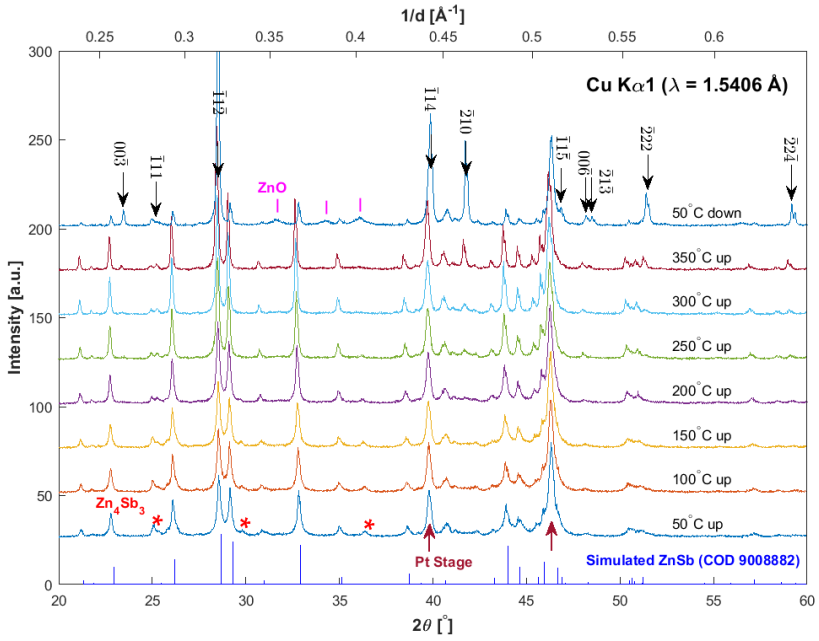

Fig. S2 The X-ray diffractogram corresponding to Fig.2 with the range in 2θ from 20° to 60°

The main phase is indexed as ZnSb, according to COD 9008882 (Version 176465, (2016) Wyckoff, R. W. G. The Structure Of Crystals). There are some additional reflections in the initial powder at room temperature, identified as Zn_4Sb_3, according to COD4001475, and attributed to incomplete diffusion or reaction during synthesis. Upon heating, Zn4Sb3 crystallizes out to ZnSb (in agreement with Ref [1]), as indicated by a decrease in the intensity of those peaks. At 300°C, i.e. Sb phase is detected in the XRD, indexed by the miller reflection. At 350°C, we could also observe some weak reflections attributed to ZnO, possibly related to spurious oxygen present in the purging.

[1] Y. Mozharivskyj, A.O. Pecharsky, S. Bud'ko, G.J. Miller, A Promising Thermoelectric Material: Zn_4Sb_3 or $Zn_{6-\delta}Sb_5$. Its Composition, Structure, Stability, and Polymorphs. Structure and Stability of $Zn_{1-\delta}Sb$, Chemistry of Materials, 16 (2004) 1580-1589.